

Research Report



The Holocene 2020, Vol. 30(3) 479-484 © The Author(s) 2019 Article reuse guidelines: sagepub.com/journals-permissions DOI: 10.1177/0959683619887418 journals.sagepub.com/home/hol

(\$)SAGE

# Holocene climate recorded by magnetic

Daniel P Maxbauer, 100 Mark D Shapley, 2,3 Christoph E Geiss<sup>4</sup> and Emi Ito<sup>5</sup>

properties of lake sediments in the

**Northern Rocky Mountains, USA** 

#### **Abstract**

We present two hypotheses regarding the evolution of Holocene climate in the Northern Rocky Mountains that stem from a previously unpublished environmental magnetic record from Jones Lake, Montana. First, we link two distinct intervals of fining magnetic grain size (documented by an increasing ratio of anhysteretic to isothermal remanent magnetization) to the authigenic production of magnetic minerals in Jones Lake bottom waters. We propose that authigenesis in Jones Lake is limited by rates of groundwater recharge and ultimately regional hydroclimate. Second, at ~8.3 ka, magnetic grain size increases sharply, accompanied by a drop in concentration of magnetic minerals, suggesting a rapid termination of magnetic mineral authigenesis that is coeval with widespread effects of the 8.2 ka event in the North Atlantic. This association suggests a hydroclimatic response to the 8.2 ka event in the Northern Rockies that to our knowledge is not well documented. These preliminary hypotheses present compelling new ideas that we hope will both highlight the sensitivity of magnetic properties to record climate variability and attract more work by future research into aridity, hydrochemical response, and climate dynamics in the Northern Rockies.

#### **Keywords**

8.2 ka, environmental magnetism, groundwater, Holocene, hydroclimate, lake sediments, Rocky Mountains

Received 13 October 2018; revised manuscript accepted 22 August 2019

#### Introduction

Lake sediments are rich archives of Holocene hydroclimate (~11.7 ka to present; for example, Dean et al., 2002; Shuman and Serravezza, 2017; Stone and Fritz, 2006). For example, Jones Lake in the central Ovando Valley of western Montana is a groundwater flow-through system with documented sensitivity to late glacial through Holocene climate variability (Shapley et al., 2005, 2008, 2009). Previous work from Jones Lake highlights the relationship of aragonite-to-calcite (a:c) ratios and  $\delta^{18}$ O of endogenic carbonate to regional hydroclimate (Shapley et al., 2008, 2009). The sensitivity of these parameters to climate, and more generally the aqueous geochemical conditions within Jones Lake, is intricately linked to the balance of groundwater inflow-outflow in the semiarid Ovando Valley, where evaporation outpaces precipitation by a  $\sim$ 2:1 ratio.

Here, we report on a previously unpublished environmental magnetic record from Jones Lake that complements existing proxy data. Despite the usefulness of environmental magnetism in reconstructions of paleoclimate and paleoenvironmental conditions from lake sediments (Geiss et al., 2003; Liu et al., 2012; Verosub and Roberts, 1995), few studies from lakes in the Rocky Mountains employ magnetic proxies. We introduce two emerging hypotheses. First, groundwater-sensitive geochemical conditions within Jones Lake appear to control rates of authigenic magnetic mineral production in lake bottom waters, providing an independent proxy of regional hydroclimate that complements a previously documented relationship between dissolved calcium flux and carbonate mineral production (Shapley et al., 2005). Second,

an abrupt increase in magnetic grain size and decrease in the concentration of magnetic minerals ~8.3 ka suggest a linkage between hydroclimate in the Northern Rocky Mountains and the 8.2 ka event in the North Atlantic (Alley et al., 1997) that is not well documented. Below, we expand on these hypotheses by interpreting environmental magnetic data from Jones Lake in conjunction with previously published geochemical and isotopic data.

### Methods

Sediment cores from Jones Lake were originally collected in 1997 and subsequently processed at the National Lacustrine Core Facility at the University of Minnesota. Details of the coring process and all non-magnetic data acquisition methods are available in

<sup>1</sup>Department of Geology, Carleton College, Northfield, MN, USA

<sup>2</sup>National Lacustrine Core Facility, University of Minnesota,

Minneapolis, MN, USA

<sup>3</sup>Continental Scientific Drilling Coordination Office, University of Minnesota, Minneapolis, MN, USA

<sup>4</sup>Department of Physics and Environmental Sciences Program, Trinity College, Hartford, CT, USA

<sup>5</sup>Department of Earth and Environmental Sciences, University of Minnesota, Minneapolis, MN, USA

#### Corresponding author:

Daniel P Maxbauer, Department of Geology, Carleton College, One North College, Northfield, MN 55057, USA. Email: dmaxbauer@carleton.edu

480 The Holocene 30(3)

Shapley et al. (2005, 2009). We update the chronology for Jones Lake by reprocessing radiocarbon dates from Shapley et al. (2009) using the Bacon package in R (Blaauw and Christen, 2018; Figure S1, available online). The updated chronology remains similar to Shapley et al. (2009) around 8.2 ka and the modeled age of the Mazama tephra remains in good agreement with independent dates (~7.6 ka; Hallett et al., 1997; Zdanowicz et al., 1999). Late Pleistocene ages are as much as 1000 cal. yr older than in the original model, because of the inclusion of a revised chronology for the Glacial Peak 'G' tephra (Kuehn et al., 2009).

In 2000, a continuous set of 2-cm resolution samples were extracted and subjected to magnetic analysis at the Institute for Rock Magnetism at the University of Minnesota. Low-field, mass-dependent magnetic susceptibility (χ, m³ kg-1) was measured using a Kappabridge KLY-1 susceptibility meter at a frequency of 920 Hz and a magnetic field strength of 300 Am<sup>-1</sup>. Magnetic susceptibility represents the contribution from all sedimentary components. However, when present even in exceedingly small mass-abundances, ferrimagnetic minerals (e.g. magnetite, maghemite, greigite) will dominate the measured χ regardless of other mineral constituents. Carbonate minerals (calcite, aragonite, and dolomite) are characterized by weak, negative  $\chi$  that is typically three to five orders of magnitude weaker than ferrimagnetic minerals. Isothermal remanent magnetization (IRM, Am<sup>2</sup> kg<sup>-1</sup>) was imparted using a direct current (DC) field of 100 mT. Anhysteretic remanent magnetization (ARM, Am<sup>2</sup> kg<sup>-1</sup>) was imparted in a peak alternating field of 100 mT in the presence of a weak DC bias field of 50 µT. ARM is most efficiently acquired by magnetic mineral grains that are in the magnetic single-domain state (SD; typical size range for SD magnetite is 30– 75 nm; Butler and Banerjee, 1975; Dunlop, 1973).

Magnetic properties reported here aim to constrain changes in concentration, grain size, and composition of magnetic minerals that are transported and deposited (via eolian deposition, runoff, or mass wasting) or formed authigenically within Jones Lake sediments. The concentration of magnetic material within sediments is reflected by changes in  $\chi$  and IRM. It is common to normalize ARM to concentration using ARM/IRM, which captures changes in the relative contribution of SD grains to remanence, independent of overall concentration (Banerjee, 1994; King et al., 1982; Liu et al., 2012; Verosub and Roberts, 1995). Considering that all magnetic parameters were acquired in relatively low magnetic fields, we will focus principally on the low-coercivity ferrimagnetic minerals magnetite (Fe<sub>3</sub>O<sub>4</sub>), maghemite ( $\gamma$ -Fe<sub>2</sub>O<sub>3</sub>), and/or greigite (Fe<sub>3</sub>S<sub>4</sub>).

#### Results

Changes in  $\chi$ , IRM, ARM, and ARM/IRM record dynamics within Jones Lake (Figure 1). Based primarily on sediment magnetic properties, we subdivide the Jones Lake record into six 'magnetic zones' (abbreviated MZ1, MZ2, etc.) that form the basis for our interpretations. Lithologic units originally described by Shapley et al. (2009) are included here in Table 1 and are shown in data figures for comparison. Mean and standard deviations for magnetic properties of each MZ are reported in Table 2. Below, we briefly highlight the main characteristics that define each MZ. Nearly identical trends are observed in  $\chi$  and IRM, both concentration-dependent parameters, and, with few exceptions, we limit our discussion below to variation in  $\chi$  and ARM/IRM for simplicity.

## Magnetic zone I (13.8–13.2 cal. kyr bp)

Basal sediments in MZ1 include sediments from lithologic units VII, VIII, and IX and represent primarily glacially derived

sediments (Shapley et al., 2009; Table 1). Magnetic properties in MZ1 are characterized by a high  $\chi$  (18.9  $\pm$  23.3  $\times$  10<sup>-8</sup> m³ kg $^{-1}$ ) and low ARM/IRM (0.032  $\pm$  0.02; see Figure 1; reported errors here and in all following instances are one standard deviation unless otherwise noted).

#### Magnetic zone 2 (13.2–11.0 cal. kyr bp)

Sediments in MZ2 are composed of olive to dark brown carbonate mud and diatom ooze (lithologic units VI and V, see Table 1; Shapley et al., 2009). Magnetic susceptibility in MZ2 decreases relative to MZ1, with an average of 3.0  $\pm$  1.3  $\times$  10<sup>-8</sup> m³ kg<sup>-1</sup>. ARM/IRM remains low in MZ2 (0.034  $\pm$  0.01). The diatom ooze in MZ2 is  $\sim$ 26 cm thick and corresponds to the Unit V anomaly identified by Shapley et al. (2009) and discussed in more detail below.

#### Magnetic zone 3 (11.0–8.3 cal. kyr bp)

MZ3 sediments are predominantly laminated carbonate mud described as lithologic unit IV by Shapley et al. (2009) (Table 1). Low  $\chi$  in MZ3 (1.9  $\pm$  0.5  $\times$  10<sup>-8</sup> m³ kg<sup>-1</sup>) is accompanied by a nearly two-fold increase in ARM/IRM relative to MZ1 and MZ2 (0.063  $\pm$  0.02) with peak values reaching ~0.1 (Figure 1).

#### Magnetic zone 4 (8.3–3.0 cal. kyr bp)

Sediments in MZ4 are olive to dark brown carbonate mud, all included in Unit III from Shapley et al. (2009) (see Table 1). The onset of MZ4 is defined here by an abrupt drop in both ARM/IRM and  $\chi$  from the last 100 years of MZ3 (8.4–8.3 cal. kyr bp) and the minima reached just prior to 8.0 cal. kyr bp at the base of MZ4  $(\sim 0.72-0.02 \text{ for ARM/IRM}; 1.87 \times 10^{-8}-0.44 \times 10^{-8} \text{ m}^3 \text{ kg}^{-1} \text{ for}$  $\chi$ ; see Figure 1). Following this ~300-year interval,  $\chi$  recovers to values similar to MZ3 ( $\sim$ 1.9  $\times$  10<sup>-8</sup> m<sup>3</sup> kg<sup>-1</sup>), punctuated by a large peak in  $\chi$  up to  $\sim 10 \times 10^{-8}$  m<sup>3</sup> kg<sup>-1</sup> within the Mazama Tephra (Figure 1), before declining over the duration of MZ3. In contrast, ARM/IRM remains low and declines through the duration of MZ4 (Figure 1). The Mazama Tephra layer represents volcaniclastic sedimentation into Jones Lake ~7.6 cal. kyr bp and overlies the transition between MZ3 and MZ4 by ~45 cm. Notably, no major lithologic changes correlate with the observed change in magnetic properties described here.

#### Magnetic zone 5 (3.0–0.8 cal. kyr bp)

Nearly all of MZ5 sediments fall into Unit III from Shapley et al. (2009), although the upper portion of MZ5 overlaps with the base of Unit II (see Figure 1; Table 1) and includes some diatom ooze in addition to carbonate mud. Concentration-dependent magnetic properties and magnetic grain size display variability (see large standard deviations for MZ5 in Table 2) but generally increase up section in MZ5 ( $\chi$  increases from ~1.0  $\times$  10<sup>-8</sup> to ~6.6  $\times$  10<sup>-8</sup> m³ kg<sup>-1</sup>; ARM/IRM increases from 0.05 to 0.11; values represent 100-year averages at the beginning and end of MZ5, respectively), reversing the early- to middle-Holocene trend of decreasing magnetic mineral concentrations and coarsening magnetic grain size (Figure 1).

#### Magnetic zone 6 (0.8–0 cal. kyr bp)

The lithology of MZ6 consists of dark greenish-brown diatom ooze with some carbonate mud toward the base of the section (Units I and II described by Shapley et al., 2009; see Table 1). ARM/IRM decreases in MZ6 from ~0.1 to ~0.08 accompanied by an increase in concentration-dependent properties ( $\chi$  increases from ~3.7  $\times$  10<sup>-8</sup> to ~23.9  $\times$  10<sup>-8</sup> m³ kg<sup>-1</sup>; values represent 100-year averages at the beginning and end of MZ6, respectively).

Maxbauer et al. 481

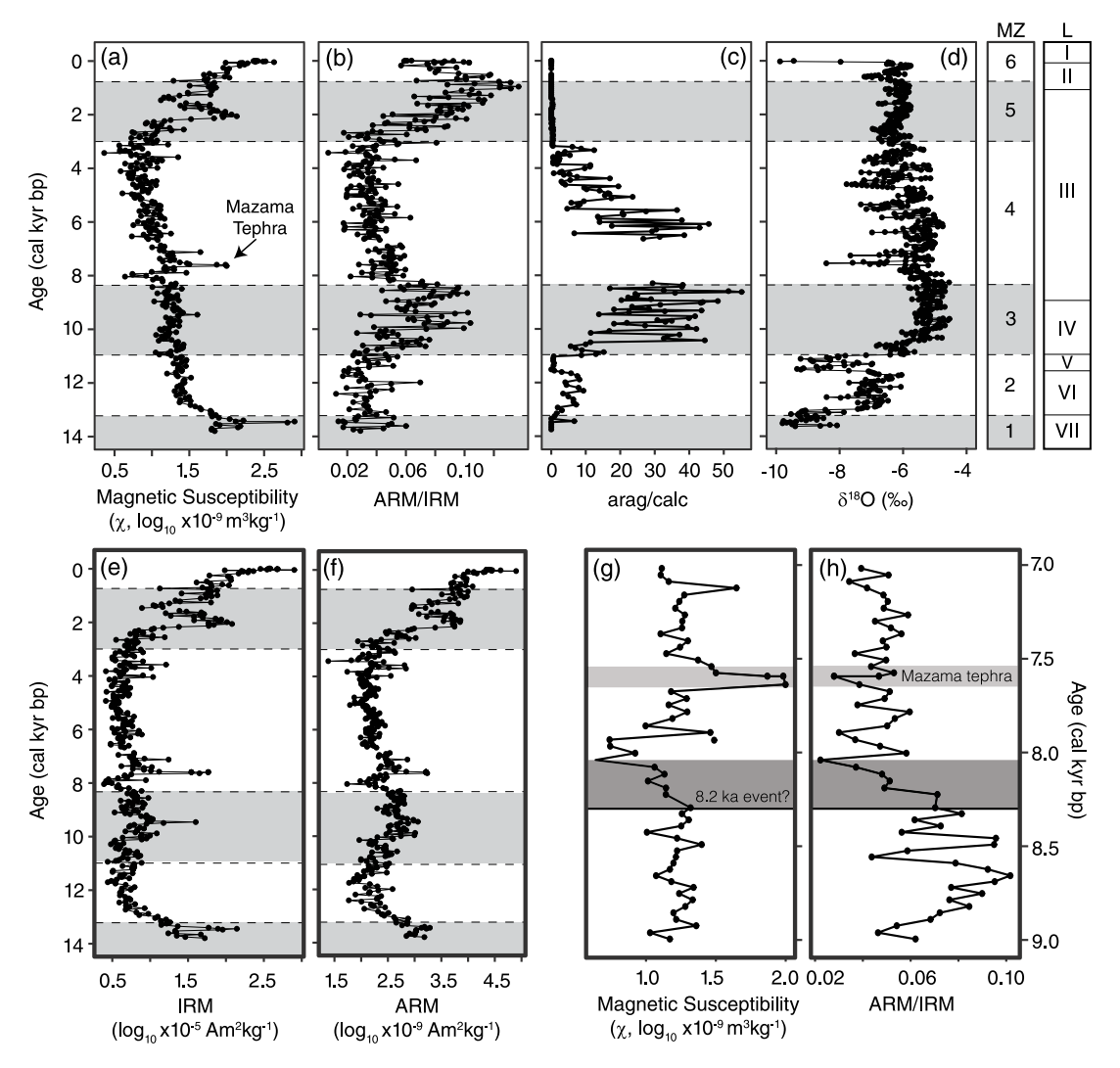


Figure 1. Magnetic, mineralogic, and isotopic data from Jones Lake. Bulk magnetic properties (a) magnetic susceptibility, (b) ARM/IRM, (e) IRM, and (f) ARM shown here along with (c) the aragonite-to-calcite ratio and (d) oxygen isotopic composition of endogenic carbonate. Aragonite-to-calcite ratios correlate with lake water salinity (more saline water corresponds to higher ratios; Shapley et al., 2009). Oxygen isotope data are measured on carbonate minerals in Jones Lake sediments. Data for (c) and (d) come from Shapley et al. (2009). Right-hand columns indicate magnetic zones (MZ; displayed as alternating gray zones in panels (a)–(f)) discussed in text and lithologic units (L) described by Shapley et al. (2009) and summarized in Table 1. Panels (g) and (h) show magnetic susceptibility and ARM/IRM, respectively, for a targeted interval across the transition from MZ3 and MZ4, denoted by solid black line. Dark gray rectangles within (g) and (h) outline period between 8.3 and ~8.0 cal. kyr bp where both magnetic properties record transitions to local minima just prior to 8.0 cal. kyr bp. Light gray rectangles outline the Mazama Tephra.

**Table 1.** Lithologic units and dominant lithologies for Jones Lake sediments. Units and descriptions from Shapley et al. (2009) with updated ages following chronology presented here. Unit labels (I–IX) follow those shown in Figure 1.

Lithologic unit	Age (cal. yr BP)	Dominant lithologies			
I	present-70	Dark greenish-brown diatom ooze			
II	70–1070	Greenish brown to gray-brown diatom ooze and carbonate mud (calcite)			
III	1070-8945	Olive to dark brown carbonate mud (aragonite)			
IV	8945-10,960	Olive to dark brown carbonate mud (aragonite) with occasional thin pyrite lamellae			
٧	10,960-11,575	Very dark brown diatom ooze			
VI	11,575–13,225	Olive to dark brown carbonate (aragonite) mud and carbonate-rich diatom ooze			
VII	13,225-13,565	Brown calcareous silt and white carbonate mud (aragonite) lamellae			
VIII	_	Greenish-gray sandy silt or silty clay with abundant pyrite			
IX	_	Gray, poorly sorted sand angular gravel			

## **Discussion and conclusions**

The sedimentary magnetic record presented here from the Northern Rocky Mountains captures both long-term and abrupt variability over the past ~14,000 years and highlights two key areas that deserve further attention. First, preliminary data reported

here support a groundwater-sourced Fe-flux model (Figure 2) for magnetic mineral authigenesis that complements a previously described Ca-flux model developed for Jones Lake and neighboring water bodies (Shapley et al., 2005) and applied to other groundwater-linked lake systems (Donovan and Grimm, 2007;

482 The Holocene 30(3)

<b>Table 2.</b> Summary	statistics fo	or magnetic zones in	Jones Lake sediments.

MZ	$\chi$ (10 <sup>-8</sup> m <sup>3</sup> kg <sup>-1</sup> )		IRM (10 <sup>-4</sup> Am² kg <sup>-1</sup> )		ARM (10 <sup>-6</sup> Am <sup>2</sup> kg <sup>-1</sup> )		ARM/IRM (10 <sup>-2</sup> )	
	Mean	SD	Mean	SD	Mean	SD	Mean	SD
I	18.9	23.3	4.51	3.63	П	4.4	3.24	1.53
2	2.95	1.26	0.62	0.34	2.14	1.51	3.37	1.12
3	1.86	0.48	0.67	0.46	4.21	2.29	6.37	2.04
4	1.3	1.49	0.63	0.78	2.42	2.82	3.89	1.22
5	3.67	3.13	3.06	2.88	27.45	27.44	7.75	3.02
6	15.39	9.97	20.15	17.93	164.12	154.46	8.71	1.9

MZ: magnetic zone; IRM: isothermal remanent magnetization; ARM: anhysteretic remanent magnetization.

Nelson et al., 2011). Second, abrupt changes in magnetic properties ~8.3 cal. kyr bp suggest a previously unrecognized linkage between the Northern Rockies and the North Atlantic during the 8.2 ka event. We expand on each of these topics below and conclude by suggesting future lines of research to address these hypotheses.

# An Fe-flux model for long-term control on the magnetic properties of Jones Lake sediments

Magnetic properties in Jones Lake sediments can be generalized into three categories. First, MZ1 is characterized by coarse magnetic grain size (low ARM/IRM) and high concentration ( $\chi$  and IRM; see Figure 1). The magnetic signature of MZ1 is consistent with coarse detrital magnetic minerals from Pleistocene tills underlying Jones Lake and is not discussed further. Second, MZ2 and MZ4 are characterized by low concentrations ( $\chi$  and IRM) and coarse magnetic grain size (low ARM/IRM; see Figure 1). Third, MZ3 and MZ5 are both characterized by a marked decrease in magnetic grain size (increasing ARM/IRM), while, in MZ3, this trend is accompanied by low concentration of magnetic minerals and, in MZ5, the concentration of magnetic minerals increases ( $\chi$  and IRM, see Figure 1).

Potential magnetic source materials to Jones Lake include eolian dust, detrital material eroded from the surrounding terrain, and authigenic formation of magnetic minerals. Magnetic properties of MZ2 and MZ4 are consistent with low rates of deposition of either eolian dust or coarse-grained detrital material that represent background conditions in Jones Lake. Increasing ARM/IRM in MZ3 and MZ5 indicates a greater contribution of SD magnetite to the overall remanence of Jones Lake sediments. Eolian and detrital sources of magnetite are typically more coarse grained (multidomain, MD) and are unlikely to drive increases in the ARM/IRM. In addition, there is no clear source of SD magnetite that may erode from nearby topsoils in the semiarid environment surrounding Jones Lake. Therefore, we suggest that the most likely source of SD magnetite is through authigenic production by magnetotactic bacteria in bottom waters (Kopp and Kirschvink, 2008), typically associated with a stratified water column where hypolimnetic oxygen is at least seasonally depleted and dissolved iron is available (Liu et al., 2012; Roberts, 2015). Contributions from SD greigite may also contribute to the magnetic record reported here, particularly in MZ4 and MZ5 where authigenic pyrite is detectable. Greigite is known to form authigenically in reducing environments associated with sulfate reduction as a precursor to pyrite (Roberts, 2015; Roberts et al., 2011).

We propose an Fe-flux model where magnetic properties of Jones Lake sediments are controlled in part by the authigenic production of magnetite and/or greigite within the hypolimnion in conjunction with variable rates of groundwater recharge and lake/ groundwater exchange. Modern groundwater inflow into Jones Lake averages  $\sim 0.3$  mg L<sup>-1</sup> dissolved iron (Shapley et al., 2005) and can reach up to 1 mg L<sup>-1</sup>, suggesting that inflow into Jones

Lake provides a flow-dependent supply of dissolved iron supporting enhanced authigenic mineral production when groundwater inflow is high. Decreased inflow of dissolved iron under low-recharge conditions in turn acts to limit rates of authigenic magnetic mineral production. In this sense, the ARM/IRM serves as an indicator for the occurrence of authigenic magnetic mineral production, while concentration-dependent properties provide a measure for the amount of authigenic production.

ARM/IRM within MZ3 increases up section with a shift toward increased salinity and more enriched  $\delta^{18}O$  of endogenic carbonate from ~11 to 8.3 cal. kyr bp, representing increased aridity in the Northern Rocky Mountains (Figure 1; Ritchie and Harrison, 1993; Schweger and Hickman, 1989; Shapley et al., 2009). The high ARM/IRM values within MZ3 (~10–8.3 cal. kyr bp) correspond with peak salinity and Holocene summer insolation for the region (~9 cal. kyr bp; Shapley et al., 2009; Figure 1). We interpret elevated ARM/IRM to be supported by relatively low rates of authigenic mineral production that are limited by groundwater mediated Fe-flux. Notably, the rates of recharge, although low, appear to have been sufficient to supply enough iron for authigenesis (supplies SD magnetite/greigite and increases ARM/IRM), albeit at very limited rates (low concentration of magnetic minerals maintained).

In the late Holocene, MZ5 (3-0.8 cal. kyr bp) coupled increases in the ARM/IRM and concentration-dependent properties (Figure 1) record increased rates of magnetic mineral authigenesis. Here, our Fe-flux model agrees well with a:c ratios indicating near persistence of freshwater in Jones Lake beginning at the base of MZ5 and sustained near-modern fluid balance beginning ~1.4 cal. kyr bp (Shapley et al., 2009). This is consistent with broad regional transitions from early- to mid-Holocene aridity toward relatively moist late-Holocene conditions across the western United States and Canada (beginning ~6–4 cal. kyr bp depending on location; Shapley et al., 2009; Shuman and Serravezza, 2017). The transition from MZ5 to MZ6 is marked by a decoupling of ARM/IRM and concentration-dependent properties (Figure 1), where coarsening of the magnetic grain size is associated with rapid increases in magnetic mineral concentration indicating additional inputs from a coarse-grained magnetic component – likely a detrital source (e.g. via erosion).

The Fe-flux model described here complements a Ca-flux model for authigenic carbonate flux (ACF) proposed by Shapley et al. (2005) for groundwater flow-through lakes (including Jones Lake). According to the Ca-flux model, wetter climates with increased rates of groundwater recharge should be associated with higher ACF in lakes with abundant dissolved inorganic carbon (DIC), and vice versa (Shapley et al., 2005). When rates of groundwater recharge were high (low a:c ratio; Figure 1) the linkage between ACF and groundwater recharge was weak (see Shapley et al., 2005). In contrast, our Fe-flux model is most clearly expressed within MZ4, suggesting sensitivity of the Fe-flux model is greatest when rates of groundwater recharge are high and lake water becomes fresh and likely more stratified (Figure 2). We

Maxbauer et al. 483

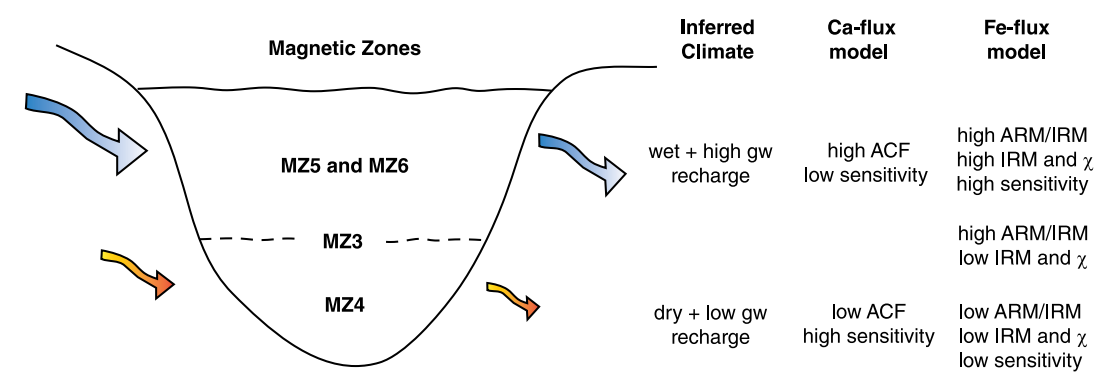


Figure 2. Schematic diagram highlighting expectations of the Fe-flux and Ca-flux models (right-hand column) with inferred climate conditions surrounding Jones Lake. Schematic at left highlights groundwater flow (arrows) for two different inferred climate states: (1) wet conditions with high rates of groundwater (gw) recharge (big blue arrows), high lake stage, and high groundwater outflow, and (2) dry conditions with low rates of recharge (small orange arrows), low lake stage, and low outflow rates. Magnetic zones corresponding to each scenario are indicated within lake schematic. Dashed line indicates intermediate conditions consistent with MZ3. Ca-flux model described briefly in text and outlined in detail in Shapley et al. (2005).

emphasize that these two models provide a set of complementary geochemical and magnetic proxies that may prove to be important tools for more fully exploiting paleorecords from flow-through lake systems under changing climates.

# Expression of abrupt climate change associated with the 8.2 ka event

Arguably the most prominent feature of the magnetic record reported here is the abrupt coarsening of magnetic grain size at the base of MZ4 ~8.3 cal. kyr bp. In addition to decreased ARM/IRM, all other magnetic properties decline close to absolute lows for the Holocene just prior to 8 cal. kyr bp (Figure 1). We suggest, similar to other studies from the mid-continent and western North America, that the change observed here in magnetic records is related to reorganization of atmospheric circulation patterns associated with reduced North Atlantic thermohaline circulation in response to surface water freshening (Alley and Ágústsdóttir, 2005; Cheng et al., 2009; Dean et al., 2002; Gavin et al., 2011; Oster et al., 2017). Low values of concentration-dependent properties and ARM/IRM (Figure 1) are consistent with aridity limiting groundwater recharge in the Jones Lake area in response to the 8.2 ka event. Arid conditions with low rates of magnetic mineral authigenesis persist until more humid conditions return ~ 3 cal. kyr bp.

#### **Acknowledgements**

We thank the research staff at both the National Lacustrine Core Facility (LacCore) and Institute for Rock Magnetism (IRM) for long-standing support and the landowners and community members from Ovando, MT, for permission to access field sites and for interest in this work. The complete dataset reported here and updated age modeling for Jones Lake are available online as supplemental materials that accompany this paper. Nina Berglund contributed analyses under CEG's supervision during a summer internship at the LacCore. This is IRM contribution 1905.

#### Funding

The author(s) received no financial support for the research, authorship, and/or publication of this article.

#### **ORCID iD**

Daniel P Maxbauer https://orcid.org/0000-0001-9736-2478

#### Supplemental material

Supplemental material for this article is available online.

#### References

- Alley RB and Ágústsdóttir AM (2005) The 8k event: Cause and consequences of a major Holocene abrupt climate change. *Quaternary Science Reviews* 24(10–11): 1123–1149.
- Alley RB, Mayewski PA, Sowers T et al. (1997) Holocene climatic instability: A prominent, widespread event 8200 yr ago. *Geology* 25(6): 483–486.
- Banerjee SK (1994) Contributions of fine-particle magnetism to reading the global paleoclimate record. *Journal of Applied Physics* 75(10): 5925–5930.
- Blaauw M and Christen JA (2018) rbacon: Age-depth modelling using Bayesian Statistics (R Package Version 2.3.4). Available at: https://CRAN.R-project.org/package=rbacon
- Butler RF and Banerjee SK (1975) Theoretical single-domain grain size range in magnetite and titanomagnetite. *Journal of Geophysical Research* 80(29): 4049–4058.
- Cheng H, Fleitmann D, Edwards RL et al. (2009) Timing and structure of the 8.2 kyr BP event inferred from δ18O records of stalagmites from China, Oman, and Brazil. Geology 37(11): 1007–1010.
- Dean WE, Forester RM and Bradbury JP (2002) Early Holocene change in atmospheric circulation in the Northern Great Plains: An upstream view of the 8.2 ka cold event. *Quaternary Science Reviews* 21(16–17): 1763–1775.
- Donovan JJ and Grimm EC (2007) Episodic struvite deposits in a Northern Great Plains flyway lake: Indicators of mid-Holocene drought? *The Holocene* 17(8): 1155–1169.
- Dunlop DJ (1973) Superparamagnetic and single-domain threshold sizes in magnetite. *Journal of Geophysical Research* 78(11): 1780–1793.
- Gavin DG, Henderson AC, Westover KS et al. (2011) Abrupt Holocene climate change and potential response to solar forcing in western Canada. *Quaternary Science Reviews* 30: 1243–1255.
- Geiss CE, Umbanhowar CE, Camill P et al. (2003) Sediment magnetic properties reveal Holocene climate change along the Minnesota prairie-forest ecotone. *Journal of Paleolimnology* 30(2): 151–166.
- Hallett DJ, Hills LV and Clague JJ (1997) New accelerator mass spectrometry radiocarbon ages for the Mazama tephra layer from Kootenay National Park, British Columbia, Canada. Canadian Journal of Earth Sciences 34(9): 1202–1209.
- King J, Banerjee SK, Marvin J et al. (1982) A comparison of different magnetic methods for determining the relative grain size of magnetite in natural materials: Some results from

484 The Holocene 30(3)

lake sediments. Earth and Planetary Science Letters 59(2): 404–419.

- Kopp RE and Kirschvink JL (2008) The identification and biogeochemical interpretation of fossil magnetotactic bacteria. *Earth-Science Reviews* 86(1–4): 42–61.
- Kuehn SC, Froese DG, Carrara PE et al. (2009) Major- and traceelement characterization, expanded distribution, and a new chronology of the latest Pleistocene Glacier Peak tephras in western North America. *Quaternary Research* 71: 201–216.
- Liu Q, Roberts AP, Larrasoana JC et al. (2012) Environmental magnetism: Principles and applications. Reviews of Geophysics 50(4): 1–50.
- Nelson DB, Abbott MB, Steinman B et al. (2011) A 6,000-yr lake record of drought from the Pacific Northwest. Proceedings of the National Academy of Sciences of the United States of America 108(10): 3870–3875.
- Oster JL, Sharp WD, Covey AK et al. (2017) Climate response to the 8.2 ka event in coastal California. *Scientific Reports* 7(1): 3886.
- Ritchie JC and Harrison SP (1993) Vegetation, lake levels, and climate in western Canada during the Holocene. In: Wright HE, Kutzbach JE and Webb T III (eds) *Global Climates Since the Last Glacial Maximum*. Minneapolis, MN: University of Minnesota Press, pp. 401–414.
- Roberts AP (2015) Magnetic mineral diagenesis. *Earth-Science Reviews* 151: 1–47.
- Roberts AP, Chang L, Rowan CJ et al. (2011) Magnetic properties of sedimentary greigite (Fe3S4): An update. *Reviews of Geophysics* 49(1): 1–46.

- Schweger CE and Hickman M (1989) Holocene paleohydrology of central Alberta: Testing the general-circulation-model climate simulations. *Canadian Journal of Earth Sciences* 26(9): 1826–1833.
- Shapley MD, Ito E and Donovan JJ (2005) Authigenic calcium carbonate flux in groundwater-controlled lakes: Implications for lacustrine paleoclimate records. *Geochimica et Cosmochimica Acta* 69(10): 2517–2533.
- Shapley MD, Ito E and Donovan JJ (2008) Isotopic evolution and climate paleorecords: Modeling boundary effects in ground-water-dominated lakes. *Journal of Paleolimnology* 391(1): 17–33.
- Shapley MD, Ito E and Donovan JJ (2009) Lateglacial and Holocene hydroclimate inferred from a groundwater flow-through lake, Northern Rocky Mountains, USA. *The Holocene* 19(4): 523–535.
- Shuman BN and Serravezza M (2017) Patterns of hydroclimatic change in the Rocky Mountains and surrounding regions since the last glacial maximum. *Quaternary Science Reviews* 173: 58–77.
- Stone JR and Fritz SC (2006) Multidecadal drought and Holocene climate instability in the Rocky Mountains. *Geology* 34(5): 409–412
- Verosub KL and Roberts AP (1995) Environmental magnetism: Past, present, and future. *Journal of Geophysical Research* 100(B2): 2175–2192.
- Zdanowicz CM, Zielinski GA and Germani MS (1999) Mount Mazama eruption: Calendrical age verified and atmospheric impact assessed. *Geology* 27(7): 621–624.